



Formation of self-organized TiO₂ nanotube arrays and its photoelectrochemical response

H Sabah Hreo¹, A Mebdir Holi^{1*}, and A Kadim Ayal²

1. Department of Physics, College of Education, University of Al-Qadisiyah, Al-Diwaniyah, Al-Qadisiyah 58002, Iraq
2. Department of Chemistry, College of Science for Women, University of Baghdad, Baghdad, Iraq

E-mail: araa.holi@qu.edu.iq

(Received 23 June 2022 ; in final form 7 March 2023)

Abstract

In this study, TiO₂ nanotube arrays (TNTAs) are produced using an efficient, low-cost, and ecofriendly environmental anodization process in an electrolyte containing Glycerin. The TNTAs were annealed for 2 hours at 500 °C. X-ray diffraction (XRD), field emission scanning electron microscopy (FE-SEM), UV-Vis diffuse reflectance spectroscopy (DRS), photoluminescence (PL), and photoelectrochemical properties (PEC) were used to analyze the sample. According to the obtained findings, the photoelectrochemical response of the TiO₂ film was accomplished with a current density (J_{ph}) of 0.196 mAcm⁻² and photoconversion efficiency of 0.14 %.

Keywords: anodization; glycerin; titanium dioxide; nanotubes arrays.

1. Introduction

Titanium dioxide (TiO₂) has gotten a lot of interest because of its unique features [1]. TiO₂ is a one-of-a-kind material because of its chemical, electrical, morphological, excellent optical properties, and high surface-to-volume ratio. TiO₂ is a one-of-a-kind substance. TiO₂ in the form of high-quality nanotube bundled structures has the potential to improve a broad range of applications' performance. It has a wide range of applications, namely solar cells [2, 3], photocatalysis [4-6], as well as gas sensors. TiO₂ (TNT) is an especially effective photocatalyst for hydrogen generation [7,8], photoelectrochemical cell since 1972 [9], and oxidation by electrocatalysis [10,11]. TiO₂'s application range continues to grow, including biosensors [12, 13]. In recent years, the fabrication of titania nanostructured has accelerated significantly [14]. Titania can be formed using various techniques, including sol-gel [15], electrodeposition [16], hydrothermal method [17], and anodization procedure [18,19]. The anodizing method is the most widely used because it is considered extremely beneficial, productive, inexpensive and simple to perform, and it does not require high temperatures. It is prepared at room temperature [19-21]. Improved TNT morphology can be achieved by adjusting the anodization time, electrolyte composition, and applied voltage [22]. The electrolyte composition [75 ml Glycerin + 25 ml water + 0.5g NH₄F] was used as an electrolyte composition in this investigation to improve the anodic

growth of self-organized TiO₂ nanotubes.

2. Experimental

2.1. Fabrication TiO₂ nanotubes

Cutting a sheet of titanium foil into (2.5x1) cm² is the first step. After fifteen minutes of treatment with ultrasonic in acetone, isopropanol, and deionized water (DI), the pieces were chemically reduced, respectively. Following that, they were immersed for 10 minutes in a solution of 6 M HNO₃ to smooth out the surface. The anodizing procedure was accomplished by a consisting cell of two electrodes configuration. The working electrode was titanium foil, with high-density graphite serving as the counter electrode. A constant two-centimeter distance was maintained throughout the experiment. After an hour of anodization at 30V, a D.C power supply (MP6010D) was used for anodizing the titanium, as shown in figure 1. Then, the anodization process was prepared using an electrolytic composition [75 ml Glycerin + 25 ml water + 0.5g NH₄F]. Following the preparation of the sample, it was washed with deionized water. The film was annealed in a thermo-oven at 500 degrees Celsius for two hours. During the electrochemical anodization of titanium in a fluoride-based electrolyte, three sequential processes occurred; see figure 1A. In the beginning, Ti is oxidized to TiO₂, thin oxide layer forms on the titanium surface, figure 1B. As a result of this reaction, fluoride anions (F⁻) are deposited on the Ti surface, resulting in a porous thin film, figure 1C.

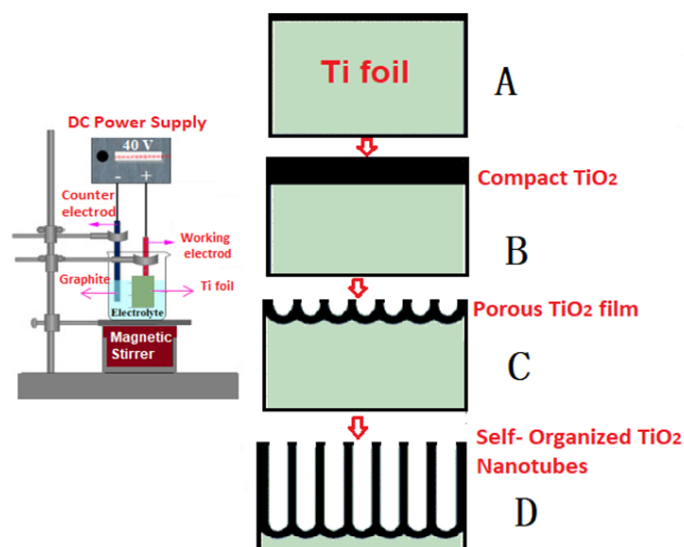


Figure 1. Schematic diagram of anodization method setup and formation steps of TiO₂ NTs; A: Ti foil (titanium metal); B: compact TiO₂ (TiO₂ thin film); C: porous TiO₂ film; D: TiO₂ NTs.

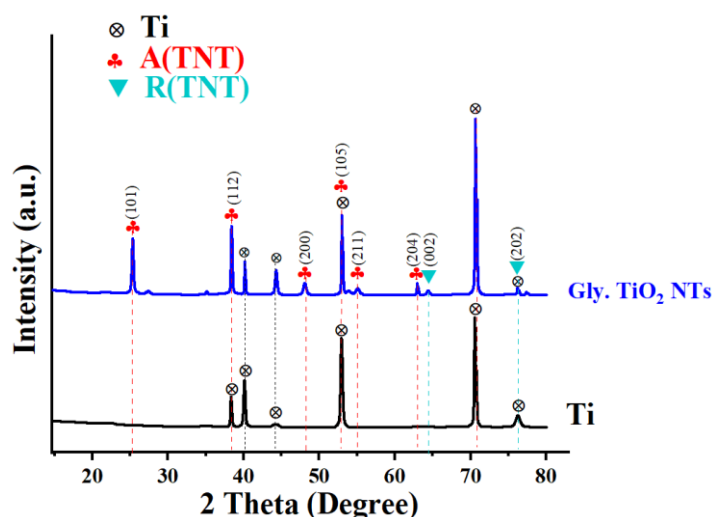


Figure 2. The XRD patterns for Ti foil and TiO₂ nanotubes.

Lastly, the surface-bound soluble titanium fluoride complex [(TiF₆)₂] dissipated slowly, creating porous TiO₂ NT structures, figure 1D.

2.2 Characterization

Shimadzu XRD-6000 Diffractometer, which has a scanning range of 20°–80°, was used to analyze the XRD patterns of the photoanode. The photo anode's morphology was analyzed utilizing a scanning electron microscope for field emission (Nano SEM 450) coupled with energy-dispersive spectroscopy (EDX). The PL emission spectra were obtained using a Perkin–Elmer LS-55 spectrophotometer. Spectra of diffuse reflectance in the UV-visible region (DRS) between 200 and 800 nm were recorded using a double beam solid-state Shimadzu TM model DUV 3700 spectrophotometer. The Kubelka-Munk theory and Tauc plot were used to analyze the bandgap energy of sample. To evaluate the PEC performance of TiO₂, a three-electrode electrochemical cell was constructed. There were three types of electrodes used in this experiment: working electrodes made of TiO₂

NTs and Bi₂S₃/TNTs samples, a platinum (Pt) counter electrode and an (Ag/AgCl) reference electrode. The electrolyte cell was obtained using mixed Na₂SO₃ (0.1 M) and Na₂S (0.1 M). Measurement of photocurrent density (Gamry Instrument framework interface with 1000 E Potentiostat/Galvanostat/ZRA) was carried out using the LSV technique. In the presence Fully Reflective Solar Simulator (SS1.6kW), the effect of the potential between (-1.2 and +1.2 V) versus Ag/AgCl at a scan rate of 20 mV s⁻¹ was found. Newport's xenon lamp simulated solar irradiation in the atmosphere and on the ground. By ASTM G173-03(2012), the lamp's output intensity matched the solar irradiance spectrum. The xenon lamp's light was focused on a quartz reaction cell (15 cm apart) with a 1 cm square working electrode area. During regular intervals, the manual chopping provided the light source, which had an irradiance of 100 mW/cm², which was equivalent to one sun lighting. The proposed TiO₂ NTs photoconversion efficiency (η%) was evaluated using the expression [23].

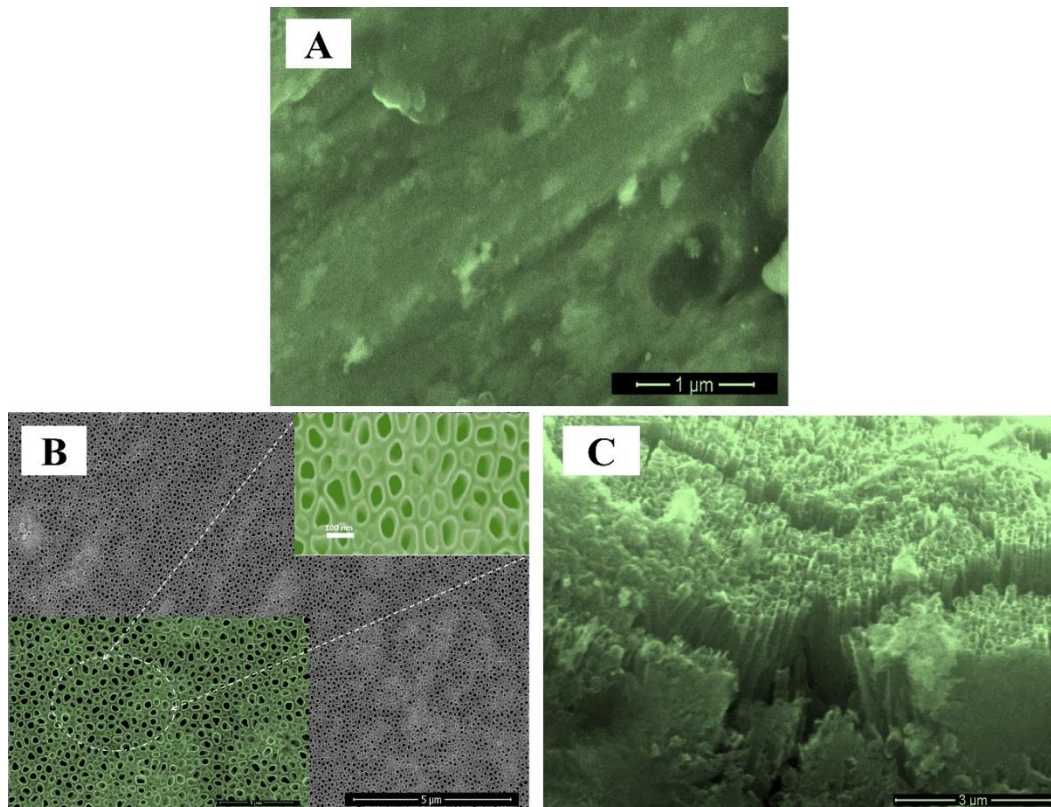


Figure 3. FE-SEM images of (A) The top-view and (B) The cross-sectional view of the TiO₂ nanotubes.

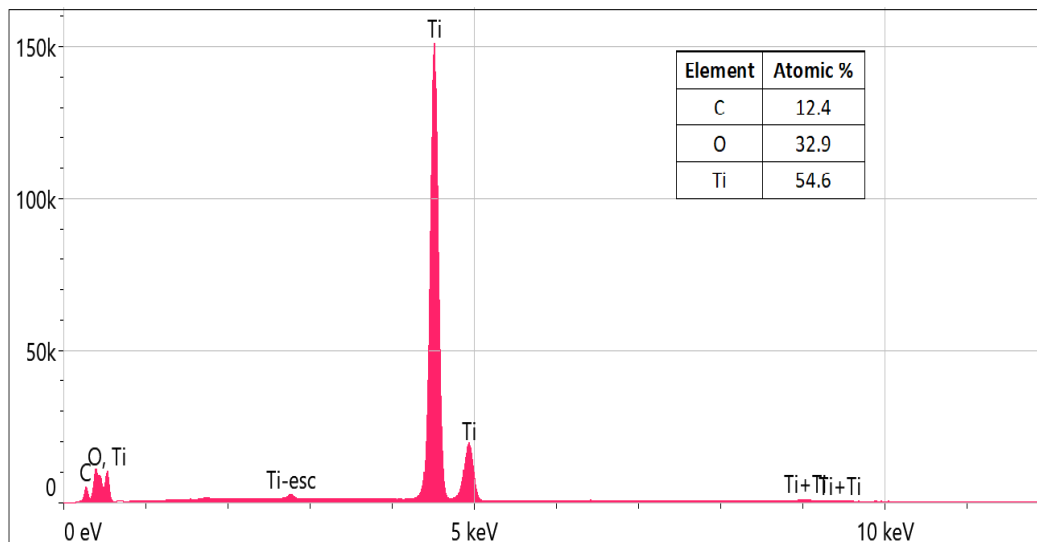


Figure 4. EDX spectra of TiO₂ NTs.

3. Results and discussion

3.1. X-ray diffraction

Figure 2 shows the X-ray diffraction patterns of Ti and TiO₂ NTs from 10° to 80° (2θ). The first pattern shows diffraction peaks corresponding to metallic Ti used as an anodizing substrate. After the Ti foil was anodized, all new peaks were matched to the standard tetragonal TiO₂ NTs rutile and anatase phases (JCPDS card number 021-1272) and (JCPDS card 021-1276). Crystallinity is sufficient to see the highest peak at 25.30° of an anatase

phase in the lattice plane (101). Debye-formula Scherers can be used to figure out the prepared sample [24]. $D=0.9\lambda/\beta\cos\theta$. 32.8 nm was the crystallite size of TiO₂ NTs and this result agree with the researcher [25].

3.2. Morphological and EDX analysis

Figure 3 depicts scanning electron microscopy images of plain Ti foil, and TiO₂ nanotubes synthesized by anodization treatment at 30V for 1 hour in a glycerin electrolyte. Results show that nanotube walls were formed in regular shapes with wide pores, as shown in figure 3B.

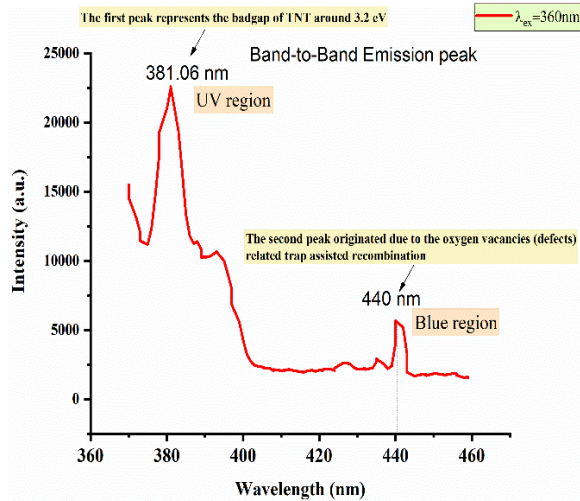


Figure 5. The PL spectra of TiO₂ NTs.

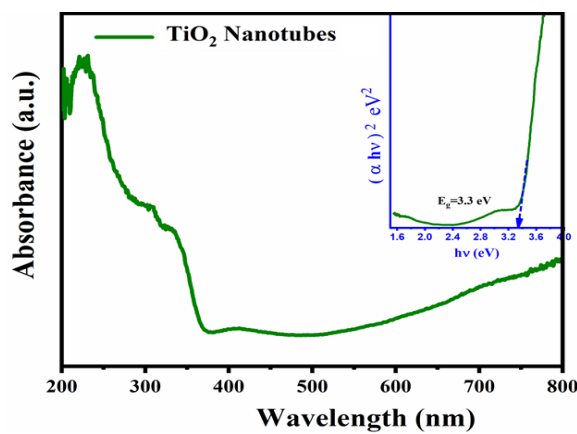


Figure 6. UV-vis diffuse reflectance spectra (DRS) for TiO₂ NTs.

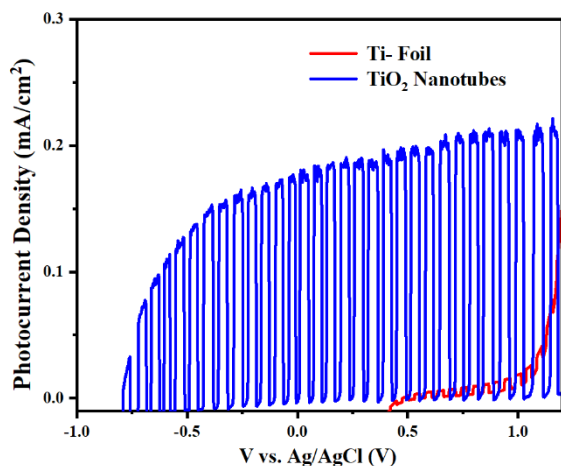


Figure 7. Linear sweep voltammograms for plain Ti foil and TiO₂ NTs obtained at a scan rate of 20 mV s⁻¹ at applied potentials ranging from -1.2 V to +1.2 V using a 100 mW cm⁻² illumination source in 0.1 M Na₂S and Na₂SO₃ electrolyte.

Table 1. shows the C.B. and V.B. values of TiO₂ NTs.

Photoanode construction	E _g (eV)	vs. NHE		vs. Vacuum	
		C.B (eV)	V.B (eV)	C.B (eV)	V.B (eV)

TiO ₂ NTs	3.3	-0.33	2.970	-4.175	-7.475
----------------------	-----	-------	-------	--------	--------

The tube diameter of the sample was measured using image analysis software (Digimizer), and the average diameter of TiO₂ NTs was found to be 100±25 nm. As depicted in figure 3C, cross-sectional image of this sample reveal a thick and aligned tube with a length of approximately 5± 300 μm, and these findings are consistent with those of the researcher [26].

The elemental composition of the sensitized TiO₂ nanotubes was determined using EDX spectroscopy. Figure 4 shows the EDX spectrum of the TiO₂ NTs sample, which confirms that it contains the components (C, O, and Ti). A small carbon peak at 0.27 keV is due to the carbon coating of the sample.

3. 3. Photoluminescence (PL) test

In figure 5, the P.L. spectrum exhibits the strongest emission peak centered at 381 nm under the excitation wavelength of 360 nm. The oxygen vacancies, surface faults, and self-trapped excitons dominate the P.L. spectrum of TiO₂ anatase [25]. The band–band transition in TiO₂ produces a peak at around 381 nm [26–27]. At approximately 440 nanometers, there is an obvious photoluminescence peak. This is most likely due to the oxygen vacancies (defects) related trap assisted recombination.

3. 4. UV-Vis spectral analysis

The UV-Vis diffuse reflectance spectra (DRS) of TiO₂ nanotubes are shown in figure 6. It illustrates the optical absorption edge of TiO₂ nanotubes, which is detected at approximately 400 nanometers, and indicates that the bandgap for TiO₂ NTs is 3.3 eV. The results show a majority of the UV light absorption by TiO₂ nanotubes occurs below 400 nm. This is because of the relative wide the bandgap of TiO₂ (3.3 eV), and these results are similar to what the researcher came up with [27].

3. 5. PEC performance

The photoelectrochemical measurements of the plain Ti and TiO₂ NTs in the electrolyte as shown in figure 7. The photocurrent responses of the Ti foil and TiO₂ NTs are around 7.4 μA/cm² and 0.196 mA/cm², respectively. To study the photoelectrochemical performance of TiO₂ NTs, it is important to understand their band edge potentials, the migration manner of photogenerated electrons and holes is strongly influenced by the band edge potential. This empirical equation can be used to predict the TiO₂ NT's valence and conduction bands [28].

$$E_{C,B} = \chi - 0.5 E_g + E_o, \quad (1)$$

$$E_{V,B} = E_{C,B} + E_g, \quad (2)$$

Here, the valence and conduction band edge potentials are E_{V,B} and E_{C,B}, and the value of χ indicates the constituent atoms' electronegativity. (E_o) is an electron's energy (- 4.5 eV), and E_g denotes the semiconductor's bandgap energy. Table 1 shows the results of the above equations, with the χ values of TiO₂ being 5.82 eV [29].

4. Conclusion

In conclusion, the use of glycerine as a solution composition in the construction of titanium dioxide

nanotube arrays TiO₂ NTs has been investigated. It was created throughout a simple anodization method in electrolytes containing small amounts of fluorine ions. The development of nanotube arrays with a photoelectrochemical response (0.196 mA/cm²) came

from the application of a TiO₂ anodic layer over a vast and continuous area on the primary Ti substrate. High-quality nanotube bundled structures made of TiO₂ have the potential to increase the performance of a number of applications, including photoelectrochemical cells.

References

1. S H Kang, W Lee, Y C Nah, K S Lee, and H S Kim, *Curr. Appl. Phys.*, **13**, 1 (2013) 252.
2. K Varghese, M Paulose, and C A Grimes, *Nat. Nanotechnol.*, **4**, 9 (2009) 592.
3. J Yuan and S Tsujikawa, *J. Electrochem. Soc.*, **142**, 10 (1995) 3444.
4. Y Guo, J Hu, H Liang, L Wan, and C Bai, *Adv. Funct. Mater.*, **15**, 2 (2005) 196.
5. G K Mor, K Shankar, M Paulose, O K Varghese, and C A Grimes, *Nano Lett.*, **6**, 2 (2006) 215.
6. A Z Faticchi et al., *Ceram. Int.*, **48**, 4, (2022) 5154.
7. Y Li, Y Xiang, S Peng, X Wang, and L Zhou, *Electrochim. Acta*, **87** (2013) 794.
8. W Krengvirat, S Sreekantan, A F M Noor, G Kawamura, H Muto, and A Matsuda, *Electrochim. Acta*, **89** (2013) 585.
9. C W Lai and S Sreekantan, *Electrochim. Acta*, **87** (2013) 294.
10. H He et al., *Electrochim. Acta*, **88** (2013) 782.
11. Y Y Song, Z. Gao, and P Schmuki, *Electrochem. commun.*, **13**, 3 (2011) 290.
12. A K M Kafi, G Wu, P Benvenuto, and A Chen, *J. Electroanal. Chem.*, **662**, 1 (2011) 64.
13. S Yu et al., *Electrochim. Acta*, **76** (2012) 512.
14. Y Lai et al., *Small*, **9**, 17 (2013) 2945.
15. M Zhang, Y Bando, and K Wada, *J. Mater. Sci. Lett.*, **20**, 2 (2001) 167.
16. Q Y Zeng, M Xi, W Xu, and X J Li, *Mater. Corros.*, **64**, 11 (2013) 1001.
17. H H Wang et al., *J. Nanomater.*, **2011** (2011).
18. L Yao, J Chen, Z Wang, and T K. Sham, *J. Phys. Chem. C*, **126**, 6 (2022) 3265.
19. J Dong et al., *ACS Appl. Mater. Interfaces*, **6**, 3 (2014) 1385.
20. R Hahn, J M Macak, and P Schmuki, *Electrochem. commun.*, **9**, 5 (2007) 947.
21. S Sreekantan, K A Saharudin, and L C Wei, *IOP Conf. Ser. Mater. Sci. Eng.*, **21**, 1 (2011).
22. H Omidvar, S Goodarzi, A Seif, and A R Azadmehr, *Superlattices Microstruct.*, **50**, 1 (2011) 39.
23. X Dong, W Huang, and P. Chen, *Nanoscale Res Lett*, **6**, 1 (2011) 1.
24. D Louër and N Audebrand, *Adv. x-ray Anal.*, **41** (1999) 556.
25. J Georgieva et al., *Appl. Surf. Sci.*, **413** (2017) 284.
26. J Gong, W Pu, C Yang, and J Zhang, *Catal. Commun.*, **36** (2013) 89.
27. A E R Mohamed and S Rohani, a review, *Energy Environ. Sci.*, **4**, 4 (2011) 1065.
28. A Helal, F A Harraz, A A Ismail, T M Sami, and I A Ibrahim, *Appl. Catal. B Environ.*, **213** (2017) 18.
29. A K Ayal et al., *J. Mater. Sci. Mater. Electron.*, **27**, 5 (2016) 5204.